Early Middle Triassic stromatolites from the Luoping area, Yunnan Province, Southwest China: geobiologic features and environmental implications

MAO LUO[1, 2], Z. Q. CHEN[2*], S. X. HU[3], C. Y. ZHOU[3], Q. Y. ZHANG[3], J. Y. HUANG[3], S. KERSHAW[4], W. WEN[3]

[1]*School of Earth and Environment, the University of Western Australia, Australia*
[2]*State Key Laboratory of Biogeology and Environmental Geology, China University of Geosciences (Wuhan), China*
[3]*Chengdu Institute of Geological and Mineral Resources, Geological Survey of China, Chengdu 610081, China*
[4]*Institute for the Environment, Halsbury Building, Brunel University, Uxbridge, UK*

ABSTRACT

Early Middle Triassic stromatolites are documented for the first time from the Guanling Formation of the Luoping area, eastern Yunnan Province, SW China. The Luoping stromatolites show six types of constructional microbial forms: ?1) typical stratified columnar structures with crinkled laminae. Dark colored laminae are composed of filamentous cyanobacteria, showing a vertical growth fabric. ?2) Laminoid fenestrae and ?3) clotted structures are also commonly present; these clotted fabrics also show an interweaved pattern of ?4) prostrate filaments, which are reflected by strong fluorescence in sharp contrast to dolomite cement in fluorescent images. ?5) Rod-like aggregates, filled with minute dolomite rhombs, are very common in laminae; they resemble present-day cyanobacterial trichome, and thus may represent fossilized cyanobacteria. ?6) Moreover, small pits, coccoid spheroids, calcified biofilms, and fibrous structures are also common in stromatolite laminae. The last two may represent calcified extra-cellular polymer secretions (EPS) that contribute to the development and lithification of stromatolites. Authigenic quartz grains are also common and may have involved biological processes in their formation. These six***<<Please can you confirm that I have correctly numbered the six types???*** functional-groups driving accretion and lithification processes of stromatolite documented in literature, both the lithified cyanobacteria/oxygenic phototrophs and sulphate-reducing bacteria (SRB) which induced microbial formation of dolomite are evident in the Luoping stromatolites, suggestive of biogenic origin. The Luoping stromatolites differ from the Early Triassic counterparts in having a great amount of biomass in filamentous cyanobacteria and SRB, whereas both anoxygenic phototrophic bacteria and SRB characterize the Early Triassic stromatolites. Abundant filamentous cyanobacteria may indicate proliferation of oxygenic phototrophs in a normal, oxic habitat. However, abundant SRB indicate sulfate reduction in a stressed habitat. Accordingly, the Luoping stromatolites, coupled with coeval unusual biosedimentary structures, indicate that the post-extinction devastated oceanic conditions may not only have prevailed in the Early Triassic but also have extended to the early Anisian (Middle Triassic) in South China, just before the full recovery of marine ecosystems in middle-late Anisian.

Keywords: stromatolite, rod aggregate, filamentous cyanobacteria, early Middle Triassic, Luoping, SW China

INTRODUCTION

As laminated microbial deposits, stromatolites are characteristics of the fossilized marine ecosystems during the Precambrian history of life (Awramik, 1971; Riding & Liang, 2005). They have also proliferated in the aftermaths of several major Phanerozoic mass extinctions and still occur in present-day oceans and salty lakes (Riding, 2006; Reitner *et al*., 2011; Mata & Bottjer, 2011). Increasing evidence shows that stromatolites provide us a unique window to probe into the history of photosynthesis, the evolution of early atmosphere and microbe-environment interactions in the geologic past (Awramik, 1992; Kah & Riding, 2007; Kershaw *et al*., 2007, 2009, 2012; Mata & Bottjer, 2011, 2012).

It is a consensus to some extent that the abundance of stromatolite deposits has undergone conspicuous perturbations since the Proterozoic (Awramik, 1971; Riding & Liang, 2005; Riding, 2006; Mata & Bottjer, 2012). This fluctuation was largely coupled with ecological turnovers through geological time, characterized by major environmental changes and ecologic crises. For instance, two of the big five Phanerozoic mass extinctions facilitated the bloom of microbialites during biotic recovery interval (?Late Devonian and end-Permian, Mata & Bottjer, 2012). This change is the result of extremely low metazoan diversity that thoroughly decreased the grazing activity and competition and meanwhile decreased bioturbation that facilitated the development of microbialites (Schubert & Bottjer, 1992; Mata & Bottjer, 2012).

The resurgence of microbial communities represented by stromatolites and other microbialites occurred through the entire Early Triassic, which correlates to the early Griesbachian, late Griesbachian, early Dienerian, and late Spathian, respectively (Pruss *et al*., 2006; Baud *et al*., 2007; Mata & Bottjer, 2012). Although the environmental range in which stromatolites developed in each stage, and paleoenvironmental implications of those biosedimentary structures have been documented in detail (Schubert & Bottjer, 1992; Sano & Nakashima, 1997; Wignall & Twitchett, 2002; Pruss *et al*., 2006; Richoz *et al*., 2005; Hips & Haas 2006; Baud *et al*., 2007; Farabegoli *et al*., 2007; Kershaw *et al*., 2011; Mata & Bottjer, 2011, 2012; Ezaki *et al*., 2012), their biogenic mechanism and functioning group structure still remain poorly understood. The functioning microbial groups that contribute to the accretions of ancient stromatolites have also long been disputed.

Moreover, the microbialites, including stromatolites occurring in the Permian–Triassic (P–Tr) boundary beds and Lower Triassic, have attracted much attention, but little has been paid on those occurring in the post-Early Triassic when marine ecosystems are believed to recover fully (Chen & Benton, 2012) except for several recent efforts (Mastandrea *et al*., 2006; Perri & Tucker, 2007). Accordingly, the relationship between microbialites development and metazoan diversity changes through the entire recovery interval remains unclear.

Here we report a new stromatolite deposit from the early Middle Triassic, an interval when ecosystems have recovered fully from the P–Tr mass extinction (Chen & Benton, 2012), of the Shangshikan section of Luoping County, eastern Yunnan Province, Southwest China (**Fig**. 1). This study aims to (1) describe microbial structure and composition of the Luoping stromatolites, (2) attempt to elucidate their accretion and formation processes, (3) compare the Luoping stromatolites with the Early Triassic examples and modern analogues, and (4) discuss in a board context their implications for interpretations of profound environmental stress and much delayed recovery of metazoans following the P–Tr mass extinction.

GEOLOGICAL SETTING AND SAMPLE CHARACTERISTICS

The studied section is located 2 km northeast of Daaozi Village, 20 km southeast of the Luoping County town, eastern Yunan Province, southwest China (Fig. 1). Paleogeographically, the Luoping area was situated at the junction between the Yangtze Platform and Nanpanjiang Basin during the Early–Middle Triassic (Feng *et al*., 1997; Enos *et al*., 2006; Hu *et al*., 2011). Therein, the stromatolite-bearing succession belongs to the second member of the Middle Triassic Guanling Formation (Zhang *et al*., 2008). Previously, the Guanling Formation was subdivided into two members. Member I is dominated by siliciclastic sediments, while Member II by micritic limestone, muddy limestone, cherty limestone, and dolomite. Stromatolites occur in the lower part of Member II, about 30 meters below the well-known Luoping biota horizon (Fig. 1). Integration of sedimentary facies analysis, paleoecology and taphonomy indicates that the Guanling Formation succession was deposited in a low energy, semi-enclosed intraplatform basin setting with influence of episodic storms (Hu *et al*., 2011).

The logged section is characterized by thick-bedded dolomitic limestone interbedded with thin- to medium-bedded limestone at lower part (0–15 m), thick-bedded dolostone alternating with medium-bedded limestone in the middle part (15–45 m), and thin- to thick-bedded limestone in the upper part (Fig. 2). Horizontal laminae are commonly present in the middle and upper parts of thick-bedded horizons. The stromatolite unit, 30 cm thick, occurs in the upper part of thick-bedded dolomitic limestone of the Member II. A thin-bedded oncoid packstone overlies the stromatolite unit.

Conodont assemblages from the overlying Luoping biota horizons, the upper part of Member II of the Guanling Formation, include *Nicoraella germancus*, *Nicoraella Kockeli* and *Cratognathodus*, indicative of a Pelsonian age of the middle Anisian (Zhang *et al*., 2009). The underlying Member I of the Guanling Formation yields bivalves *Myophoria (Costatoria) goldfussi mansuyi* Hsü, *Unionites spicatus* Chen, *Posidonia* cf. *pannonica* Moj, and *Natiria costata* (Münster) and pronounced clay beds, which have been regarded as correlation markers of the base of the Anisian in southwest China (Enos *et al*., 2006; Zhang *et al*., 2009). The stromatolite unit therefore is of middle Anisian age.

METHODS

Both polished slabs and petrologic thin sections were used to examine internal fabrics and diagenetic features of the stromatolites. Fresh samples and polished slabs were prepared separately for a micro-analysis under scanning electron microscope (SEM). These samples were cleaned first by diluted water and then etched with 0.5 % chloride acid for 3-5 hours, followed by a second rinse using diluted water and ethyl alcohol. Some samples for SEM analysis were polished with 200 mesh diamond dust before chemical etching and cleaning. Samples were all coated with gold for a surface texture analysis and energy dispersive X-ray spectrometry (EDS) analysis using VP FESEM 1555 in the Centre of Microscopy, Characterization and Analysis (CMCA) at the University of Western Australia, Australia.

Fluorescent imaging analysis was undertaken to detect signals of organic matter in stromatolites using fluorescent microscopy in the State Key Laboratory of Biogeology and Environmental Geology, China University of Geosciences (Wuhan), China. Terminology and methods documenting stromatolite microfabrics follow Shapiro (2000) who observed

microbial fabrics at three different scopes***<<I am not fully understanding "scopes"; do you mean "magnifications"??? Please check***.

RESULTS

Non-stromatolite facies associations

The substrate of stromatolites comprises dolomitic bioclastic limestone, which has wackestone texture (Fig. 3A). Fossil fragments are mostly recrystallized and altered to coarse dolomite. The matrix is dominated by microbial limestone. Inter-stromatolite facies are dominated by oncoidal packstone-wackestone, yielding fragmented stromatolites and various shell fragments of bivalves, foraminifers and crinoids, which are mostly coated with microbial micrite and microbes to form various oncoids (Fig. 3B, C). Bioclasts and peloids are common. Capping facies of the stromatolites is composed of bioclastic packstone-wackestone and oncoidal packstone. The former is dominated by microbial filaments, clotted structures and microbial micrite with few recrystallized fossil fragments (Figs 3D, 4E), while the latter is characterized by abundant irregularly shaped oncoids (Fig. 4D).

Mega-, macro-and mesostructures of Luoping stromatolites

In outcrop, stromatolites show typically stratified columnar structures, contrasting with the surrounding rocks (Fig. 2A, B). In cross section, stromatolitic laminae are crinkled and laterally linked. These initial, space-linked hemispheroids pass into discrete, vertically-stacked hemispheroids (Fig. 2A). Discrete, vertically stacked hemispheroids composed of closely-linked hemispheroidal laminae are also occasionally present (Fig. 2B).

In polished slabs, the crinkled to columnar laminae are characterized by vertically-stacked hemispheroids passing into close-linked hemispheroids by upward growth (Fig. 2C). In plan view, discrete spheroids show a structure that consists of concentrically-stacked hemispheroids (Fig. 2D, E).

Microstructures

Under optical microscope, planar and domal stromatolites are characterized by undulating laminations with a few skeletal grains (Fig. 4A). The overlying oncoidal packstone caps the laminated stromatolites (Fig. 4D), with a distinct contact. Stromatolite laminae comprise alternations of light-grey microsparitic dolomite with dark-grey micritic dolomite. Dark colored laminae, 1 mm thick, are composed of filamentous cyanobacteria, which show an up-straight growth fabric (Figs 4B–C, 5A–C). Filaments interweave to form consortia (Figs 4B–C, 5A–C). Individual calcified cyanobacterial sheaths have microsparitic molds and the margins are defined by dark grey micrite possibly rich in organic matter (Figs 4C, 5B–C). The sheaths are 10–20 μm in diameter. Light grey laminae are 2–5 mm thick and contain laminoid fenestrae (Figs 4A, 5A). The irregularly shaped clotted structures are commonly present in some interlayed areas (Figs 4A, d, 5D–F). These clotted fabrics also exhibit interweaved patterns of prostrate filaments (Fig. 5D–F).

Under fluorescent microscope, clotted areas composed of prostrate filaments showed strong fluorescence in both blue and green light, which contrasted with the coarse grained dolomite

cement (Fig. 6A–C). This agrees with the interpretation that micritized filaments might be the fossilized bacteria, which are rich in organic matters. The micritized areas within dark laminae, although lacking the well-preserved filaments, also showed a strong fluorescence (Fig. 6D–F), strengthening that filamentous cyanobacteria may exist in organically rich dark laminae.

Rod aggregates

Under SEM, the well-preserved, rod-like aggregates are commonly present in stromatolite laminae (Fig. 7B–E). Individual rods are straight to slightly curved in outline (Fig. 7B, C, F). They are mostly scattered in laminae, but aggregate locally to form rod colonies (Fig. 7D–F). When clustered together, these trichome-like rods interweave to form 3-dimensional consortia, which resemble remarkably the cyanobacterial trichome from present-day microbial mats (Brigmon *et al*., 2008, fig. 5, 14A). Rod-like filaments are 4.6–18 μm in diameter, with an average diameter of 8.5 μm based on measurement of 26 individual rods. In plan view, each rod normally shows a centre filled with minute dolomite rhombs (Fig. 7D). Vertical cross sections show dolomite grains are all euhedral rhombs (Fig. 7B–D, F), no more than 5 μm long. They formed a mosaic fabric forming rods or are intensively stacked, with rhombs interpenetrating one another (Fig. 7B, C). Dolomitic rods are usually well-orientated, which are in sharp contrast to the surrounding dolomite grains that are irregularly arranged. The contact between the two is rather distinct (Fig. 7B, C).

Small, rounded pits (15–25 μm in diameter) and coccoid spheroid (12 um in diameter) are also very common in laminae (Fig. 7G–H). They resemble superficially spherical bodies and form small clusters. These tiny pits are also analogues to modern examples of mineralized capsules from the Lake Vai Si'I, Tonga (Kaźmierczak & Altermann, 2002, fig. 1B, D) in all observed aspects.

The rod-like filaments are well-preserved with a pronounced sheathed mold (Fig. 8), although the centres were usually filled with coarse dolomite grains. The sheathed layer is 2 μm thick. In particular, nano-sized dolomite grains are in proximity with those dolomite rhombs composing rods. This might indicate that rod might be composed of nano-sized dolomite grains, which further recrystallized to form micron-sized rhombs.

EPS remnants

Another feature typifying the dolomite rod aggregates is the common presence of calcified biofilms (Fig. 9A) and fibrous structures (Fig. 9B, C, E). These mucilaginous materials cover or attach to minute dolomite rhombs. Biofilms are commonly present and usually preserved as coalescing filaments that bound various rod aggregates together (Fig. 9C, D, E). They may represent the calcified extra-cellular polymer secretions (EPS) produced by microbial communities that contribute to the development and lithification of stromatolites (Dupraz *et al*., 2005, 2009).

Authigenic quartz

Quartz grains are also pronounced in stromatolite microstructures. They coexist with minute dolomite rhombs within laminae. Quartz crystals are characterized by euhedral outlines and pronounced crystal structures on both ends (Fig. 9F). Quartz grains vary from silt to fine sand in size and occur over the stromatolite laminae. They also cluster occasionally or touch other fossil skeletons (Fig. 9F) with the undulated contact between quartz and fossil skeletons.

Euhedral quartz crystals show no signs of abrasion, scatter in stromatolite laminae and do not concentrate to form layers or horizons, which are typical of detrital quartz grains. These crystals therefore are likely authigenic in origin, showing no sign of transportation.

DISCUSSION

Geobiologic process of the Luoping stromatolites

Increasing evidence shows that various microbial colonies co-existed in different layers within stromatolite laminae and they initiated various metabolic processes coupling with one another (Dupraz *et al*., 2005). These bio-reactions controlled bio-carbonate precipitation and dissolution and subsequently drove accretion and lithification of stromatolite. Six typical functional-groups have been considered as key components driving those processes (Visscher & Stolz, 2005; Dupraz & Visscher, 2005, Dupraz *et al*., 2009). They are (i) oxygenic phototrophs (cyanobacteria) that use light energy to generate adenosine triphosphate (ATP) and fix carbon; (ii) anoxygenic phototrophs that use reduced sulfur to generate ATP; (iii) aerobic heterotrophic bacteria that consume organic carbon and O_2 for a respiration and living, while producing CO_2 needed in photosynthesis at the same time; (iv) fermenters that use organic carbon or sulfur compounds for a metabolism; (v) anerobic heterotrophs (predominantly SRB) that consume organic carbon to carry out sulfate reduction process; (vi) sulfide oxidizing bacteria that oxidize reduced sulfur by consuming O_2 while fixing CO_2. All bio-reactions make a semi-closed system in stromatolite that enables to maintain an efficient element cycling and highest metabolic rates (Visscher *et al*., 1998; Dupraz *et al*., 2005). The above bio-reaction processes were summarized based on modern stromatolites because prolific living bacteria consortia and biosignatures can be directly detected and observed *in situ*. Biosignatures from ancient examples are crucial in understanding genesis and accretion process of stromatolites in geological past. Herein, the Luoping stromatolites provide evidence for at least two key functioning groups involved in stromatolite accretion processes.

Lithified cyanobacteria and oxygenic phototrophs in stromatolites

Filamentous rod aggregates are very common in dark laminae of the Luoping stromatolites. Such well-arranged, rod-like aggregates of minute rhombic dolomite crystals have also been observed from the Pliocene lacustrine dolomite of La Roda, Spain (Garcia del Cura *et al*., 2001) and Miocene carbonate stromatolite in the Caltanissetta Basin of Sicily, Italy (Oliveri *et al*., 2010). The Spanish dolomite aggregates have been interpreted as biogenic structures (Garcia del Cura *et al*., 2001), while the Italian example of elongate filaments as the fossilized *Beggiatoa*-like sulfur bacteria (Oliveri *et al*., 2010). The Luoping rod aggregates therefore are likely the fossilized forms of cyanobacteria. This inference is also reinforced by similarity in size and interweaving pattern between the Luoping rods and fossilized cynaobacteria in literature (Seong-Joo *et al*., 2000; Golubic *et al*., 2000) and modern stromatolites from hypersaline lakes (Kaźmierczak *et al*., 2011). If so, these fossilized cyanobacteria represent primary producers that constructed the Luoping stromatolites. Therein oxygenic phototrophs may have contributed to carbon fixation and oxygen production and facilitated other microbial-functioning groups to conduct their metabolism.

Microbial dolomite formation and sulfate-reduced bacteria (SRB) in stromatolites

In the Luoping stromatolites, bacteria sulfate reduction and a microbial process mediating dolomite precipitation in subsurface environment (*sensu* Wright & Wacey, 2005) have not been directly observed. However, several lines of evidence show the existence of the SRB-induced microbial formation of dolomite in the Luoping stromatolites.

As stated above, the Luoping stromatolites have abundant minute rhombic dolomites that formed rod aggregates. Comparable structures have been interpreted as a result of microbial metabolism caused by bacteria sulfate reduction elsewhere (Garcia del Cura *et al*., 2001; Oliveri *et al*., 2010). Moreover, authigenic quartz in conjunction with minute rhombic molds is also commonly present in the stromatolite. The formation of euhedral quartz crystals has been interpreted as a result of lowered pH by sulfide oxidizing, in which sulfide was produced by sulfate reduction (Chafetz & Zhang, 1998). As a result, growth of euhedral authigenic quartz indicates the bacteria sulfate reduction and sulfide oxidation processes, which facilitated adjacent minute dolomite rhombs to form rod aggregates. It should also be noted that the possibility that those euhedral quartz originated from volcanism cannot be ruled out since volcanism has been very active through the Early-Middle Triassic in South China (Chen & Benton, 2012).

Minute dolomite rhomb interacted closely with fibrous materials and biofilms. Mucilaginous materials or biofilms covered minute rhombic dolomite grains and coalesced different rods individuals to form reticular structure (Fig. 9B–C, E). Fibrous fabrics have been usually interpreted as the remains of deflated exopolymeric substances (EPS), which boost the formation of unstructured fibrils and deflated films on dolomite grain surfaces (Renaut *et al*., 1998).

In fact, EPS have played a crucial role not only in calcium carbonate precipitation (Riding, 2000; Dupraz *et al*., 2004, 2005; Braissant *et al*., 2007; Bontognali *et al*., 2010), but also in dolomitization process in subsurface condition (Bontognali *et al*., 2010; Krause *et al*., 2012). This is because EPS might have served as a template to induce the dolomite formation directly from solutions and exopolymeric substances were visualized as an alveolar organic network, within which precipitation of dolomite was initiated (Bontognali *et al*., 2010). The ability of EPS to preferentially bind Mg and Si over Ca may play a crucial role in overcoming the kinetic barriers that prevent nucleation of dolomite at subsurface environment (Bontognali *et al*., 2010). Krause *et al*. (2012) further emphasized that precipitation of a high Mg/Ca molar ration carbonate crystal that associated with EPS excreted of SRB provide templates for nucleation of stoichiometric dolomite. SRB therefore played an important role in this process.

In the Luoping stromatolites, EDS analysis of two different dolomite components (Fig. 10A, B) suggests that the growth of dolomite rod aggregates follows the above EPS template mechanism. Minute dolomite rhombs are rich in Mg and Ca, with small percentage of Si. This is probably due to the subsequent Ca incorporation within the previously formed Si-Mg phase that was encapsulated by EPS matrix. In addition, the intimate relationship between biofilms, representing EPS remnants, and rod aggregates of dolomite also supports the view that EPS may have played an important role in the formation of primary dolomite.

It is also true that minute dolomite rhombs, forming the filamentous rods, in the Luoping stromatolites show neither “bacterial shapes” nor dumbbell forms, both of which usually indicate microbial formation of dolomite (Vasconcelos *et al*., 1995; Vasconcelos & Mckenzie, 1997; Garcia del Cura *et al*., 2001). This is probably, in part, due to progressive dolomitization and subsequent recrystallization during shallow and deep burial that commonly obliterated the primary dolomite microfacies (Mastandrea *et al*., 2006) or an

alteration from diagenetic self-organization (Wright, 1999). This neomorphic process of crystal growth is not uncommon; as such alterations have been documented from Holocene marine dolomites (Gregg *et al.*, 1992) and in microbial mats of the coastal Sabkha of Abu Dhabi (Bontognali *et al*., 2010).

Accordingly, abundant rod aggregates might indicate active metabolism of SRB in stromatolite. Through excreting EPS in great abundance, SRB induced the formation of dolomitized rod aggregates and entailed the fossilization of filamentous cyanobacteria (Bontognali *et al*., 2010).

Biogenetic origin of the Luoping stromatolite

As outline above, two main microbial functioning groups: fossilized filamentous cyanobacteria sheath and SRB represented by copious rods aggregates composed of minute dolomite grains in laminae are distinct in the Luoping stromatolites. They both might represent the most active microbial communities in stromatolite ecosystem. Other important microbial components include aerobic heterotrophs, anoxygenic phototrophs and sulfide oxidizing bacteria. They may have also contributed to stromatolite accretion.

Moreover, laminoid fenestrae are also rich in the Luoping stromatolite (Figs 4A–C, 5A). Reid *et al*. (2003) treated the comparable fenestrae as the space that was initially occupied by organic framework of accreting mat. Other microbial processes such as aerobic respiration, aerobic sulfide oxidation, and fermentation would also result in dissolution of $CaCO_3$ and degradation of organic matter in framework and might have induced the subsequent formation of those laminoid fenestrae (Ezaki *et al*., 2012). As such, all lines of evidence indicate that the Luoping stromatolite is biogenic in origin.

Comparison with Early Triassic stromatolites

Microbialites including stromatolites, thrombolites and other unknown forms characterize the P–Tr boundary (PTB) successions in many shallow marine facies sections (Kershaw *et al*., 2012). They are interpreted as a sedimentation phenomenon related to the severe end-Permian mass extinction. However, stromatolites are not common among the PTB microbialites. Of these, one PTB stromatolite deposit was described from the Chongyang section of southern Hubei Province, South China (Yang *et al*., 2011). Unlike the Luoping stromatolites having abundant fossilized cyanobacteria, the Chongyang stromatolites are dominated by occoid bacteria (Yang *et al*., 2011). Other PTB stromatolites have also reported from Cürük Dag of Turkey, Bükk Mountains of Hungary, Hambast of Iran (Kershaw *et al*., 2011, 2012). Their microbial compositions remain unclear because no geomicrobiological studies are available.

The younger Early Triassic stromatolites have also been reported from Japan, Germany and South China (Sano & Nakashima, 1997; Paul & Peryt, 2000; Paul *et al*., 2011; Ezaki *et al*., 2012). A detailed study of their geomicrobiology and microbiology lagged behind their ecologic studies. Ezaki *et al*. (2012) detected that the late Early Triassic stromatolites from South China were constructed by the activity of sulphate–reducing or anoxygenic phototrophic bacteria. Its microbial composition is related to the inhospitable anoxic/sulphidic marine conditions prevailing in the Early Triassic. The deleterious environment might have prevented growth of oxygenic phototrophs such as cyanobacteria but enhanced the accretion of anoxygenic phototroph that utilized copious HS^- in stressed habitats for a metabolism (Ezaki *et al*., 2012).

The early Middle Triassic stromatolites therefore are different from the late Early Triassic counterparts in terms of the functioning microbial groups. The former are characterized by a great amount of biomass in filamentous cyanobacteria and SRB, while the latter by anoxygenic phototrophic bacteria and SRB (Ezaki *et al*., 2012).

Other Early Triassic stromatolites have also been reported worldwide (see reviews by Pruss *et al*., 2006; Baud *et al*., 2007; Kershaw *et al*., 2012). Nevertheless, genesis of other Early Triassic stromatolites remains unclear, although they are generally believed to be biogenic in origin.

Implications for devastated post-extinction oceanographic conditions extending to the Middle Triassic

Early Triassic stromatolites have been reported in various localities around the world (Schubert & Bottjer, 1992; Sano & Nakashima, 1997; Pruss *et al*., 2006; Richoz *et al*., 2005; Hips & Haas, 2006; Farabegoli *et al*., 2007; Kershaw *et al*., 2011; Mata & Bottjer, 2012). They are major components of the post-extinction microbialites. Although the debate on genesis of the P–Tr microbialites still continues (Kershaw et al., 2007, 2012; Mata & Bottjer, 2012), biogeochemical signals show that microbes were extremely abundant immediately after the end-Permian extinction even in the microbialite-free areas such as Meishan (Xie et al., 2005). Thus, other factors such as highly saturated carbonate conditions in the post-extinction oceans (Grotzinger and Knoll, 1995; Woods et al., 1999; Pruss et al., 2005; Riding, 2005; Riding and Liang, 2005 Pruss et al., 2006; Baud et al., 2007) combined with factors unfavorable to most normal skeletal organisms may have facilitated the formation of the P–Tr microbialites. Kershaw *et al.* (2007) and Woods *et al.* (2007) also emphasized that the elevated carbonate supersaturation caused by the upwelled $CaCO_3$-rich anoxic waters mixed with aerated surface waters may be the key driver for the P–Tr precipitation of microbialites. Thus, the microbialite ecosystem has very special biogeochemical conditions that related to the P–Tr mass extinction (Mata & Bottjer, 2012).

More recently, Ezaki *et al*. (2012) confirmed that such stressed conditions have extended to the late Early Triassic on the basis of detailed geobiologic studies of an Olenekian stromatolite from South China. These authors considered that the late Early Triassic stromatolite grew in the inhospitable anoxic/sulphidic marine conditions. Interpretation of such deleterious oceanic conditions throughout the Early Triassic have also been strengthened by other anachronistic facies such as microbialites (Mary & Woods, 2008; Mata & Bottjer, 2012), sea-floor carbonate precipitation (Woods *et al*., 1999), vermicular limestone (Zhao *et al*., 2008), and giant ooids (Li *et al*., 2012; Woods, 2012) as well as extremely warm seawater temperature (Sun *et al*., 2012).

As stated above, the Luoping stromatolite ecosystem was characterized by a great amount of biomass in filamentous cyanobacteria and SRB. It is superficially similar to those of the Type II stromatolite described from the Highborne Cay, Bahamas (Decho *et al*., 2005). The latter is characterized by the higher biomass within layer 1 and layer 3 in stromatolites, corresponding to the content peaks of cyanobacteria and SRB, respectively (Reid *et al*., 2000; Decho *et al*., 2005). Abundant filamentous cyanobacteria may indicate the proliferation of oxygenic phototrophs in a normal, oxic habitat. However, abundant SRB indicate sulfate reduction in a stressed habitat. Consequently, the Luoping stromatolites also indicate an environmentally stressed ecosystem that may have been devastated by the same disaster

causing the P–Tr biocrisis (Ezaki *et al*., 2008, 2012). This inference is reinforced by the presence of sea-floor carbonate precipitation, microbialite, ether lipids, and archaeol ***<<do you mean "archaea"?? Please check*** from the early-middle Anisian of the Qingyan area of the same oceanic basin (Chen *et al*., 2010a; Saito *et al*., 2013). The first two unusual sedimentary structures are characteristic of Early Triassic devastated environments (Woods *et al*., 1999; Kershaw *et al*., 2012; Mata & Bottjer, 2012), while the latter two biomarker proxies derived from sulfate-reducing bacteria (SRB), which are restricted to anaerobic habitats, indicating that anoxic condition expanded in the depositional and/or water-column environment during the early Middle Triassic in South China (Saito *et al*., 2013).

Accordingly, the Luoping stromatolites, coupled with coeval unusual sedimentary structures, indicate that the devastated oceanic condition may not only have prevailed in the entire Early Triassic (Chen *et al*., 2010b; Algeo *et al*., 2011; Chen & Benton, 2012) but also have extended to the middle Anisian (Middle Triassic), just before the full recovery of marine ecosystems in middle–late Anisian (Chen & Benton, 2012).

CONCLUSION

The Luoping stromatolites show the typically stratified columnar structures with crinkled laminae. Dark colored laminae are composed of filamentous cyanobacteria, showing an up-straight growth fabric. Laminoid fenestrae and clotted structures are also commonly present. These clotted fabrics show interweaved pattern by prostrate filaments, which are reflected by strong fluorescence in sharp contrast to dolomite cement on fluorescent images. The rod-like aggregates, filled with minute dolomite rhombs, are very common in laminae. They resemble present-day cyanobacterial trichomes, and thus may represent fossilized cyanobacteria. Moreover, small pits, coccoid spheroids, calcified biofilms, and fibrous structures are also common in stromatolite laminae. The last two may represent the calcified extra-cellular polymer secretions (EPS) that contribute to the development and lithification of stromatolites. Authigenic quartz grains are also abundant and indicate biologic involvement in their formation process. Lithified cyanobacteria/oxygenic phototrophs and SRB-induced microbial formation of dolomite are distinct during the growth of stromatolites, strengthening the view that the Luoping stromatolites are biogenic in origin. The Luoping stromatolites differ clearly from the Early Triassic counterparts in having abundant filamentous cyanobacteria and SRB, whereas the latter possess anoxygenic phototrophic bacteria and SRB. Abundant filamentous cyanobacteria may indicate the proliferation of oxygenic phototrophs in a normal, oxic habitat. However, abundant SRB indicate sulfate reduction in a stressed habitat. The Luoping stromatolites, coupled with coeval unusual biosedimentary structures, indicate that the devastated oceanic conditions may not only have prevailed in the entire Early Triassic but also have extended to the middle Anisian (Middle Triassic), just before the full recovery of marine ecosystems in middle-late Anisian.

ACKNOWLEDGEMENTS

The author wishes to thank Peter Ducan and Lyn from CMCA, the University of Western Australia for their guidance and helpful suggestions in sample preparation and SEM imaging. This study is supported by the 111 Program of China (B08030 to SCX), a National Natural Science Foundation grant (No 41272023 to ZQC), and a grant-in-aid for the study on the

Permian−Triassic mass extinction and recovery from the State Key Laboratory of Biogeology and Environmental Geology, China University of Geosciences (to ZQC). It is a contribution to the IGCP 572 “Permian−Triassic ecosystems”.

REFERENCES

Algeo T, Chen ZQ, Fraiser ML, Twitchett RJ (2011) Terrestrial–marine teleconnections in the collapse and rebuilding of Early Triassic marine ecosystems. *Palaeogeography, Palaeoclimatology, Palaeoecology* **308**, 1–11

Awramik SM (1971) Precambrian columnar stromatolite diversity: reflection of metazoan appearance. *Science* **174**, 825–827.

Awramik SM (1992) The oldest records of photosynthesis. *Photosynthesis Research* **33**, 75–89.

Baud A, Richoz S, Pruss S (2007) The lower Triassic anachronistic carbonate facies in space and time. *Global and Planetary Change* **55**, 81–89.

Bontognali TR, Vasconcelos C, Warthmann RJ, Bernasconi SM, Dupraz C, Strohmenger CJ, Mckenzie JA (2010) Dolomite formation within microbial mats in the coastal sabkha of Abu Dhabi (United Arab Emirates). *Sedimentology* **57**, 824–844.

Braissant O, Decho AW, Dupraz C, Glunk C, Przekop KM, Visscher PT (2007) Expolymeric substances of sulfate-reducing bacteria: interactions with calcium at alkaline pH and implication for formation of carbonate minerals. *Geobiology* **5**, 401–411.

Brigmon R, Morris P, Smith G (2008) Evaporite microbial films, mats, microbialites and stromatolites. In *Links between Geological Process, Microbial Activities & Evolution of Life* (eds Dilek Y, Furnes H, Muehlenbachs K). Springer Press, pp. 197–235.

Chafetz HS, Zhang JL (1998) Authigenic euhedral megaquartz crystals in a quaternary dolomite. *Journal of Sedimentary Research* **68**, 994–1000.

Chen ZQ, Benton MJ (2012) The timing and pattern of biotic recovery following the end-Permian mass extinction. *Nature-Geoscience* **5**, 375–383.

Chen ZQ, Chen J, Fraiser ML (2010a) Marine ecosystem changes from latest Permian to Middle Triassic in the Qingyan area, Guizhou, southwest China. *Journal of Earth Science* **21**(Special Issue), 125–129.

Chen ZQ, Tong JN, Liao ZT, Chen J (2010b) Structural changes of marine communities over the Permian–Triassic transition: ecologically assessing the end-Permian mass extinction and its aftermath. *Global and Planetary Change* **73**, 123–140.

Decho AW, Visscher PT, Reid RP (2005) Production and cycling of natural microbial exopolymers (EPS) within a marine stromatolite. *Palaeogeography, Palaeoclimatology, Palaeoecology* **219**, 71–86.

Dupraz C, Visscher PT, Baumgartner LK, Reid RP (2004) Microbe-mineral interactions: early carbonate precipitation in a hydpersaline lake (Eleuthera Island, Bahamas). *Sedimentology* **51**, 745–765.

Dupraz C, Visscher PT (2005) Microbial lithification in marine stromatolites and hypersaline mats. *Trends in Microbiology* **13**, 429–439.

Dupraz C, Reid RP, Braissant O, Decho AW, Norman RS, Visscher PT (2009) Process of carbonate precipitation in modern microbial mats. *Earth-Science Reviews* **96**, 41–162.

Enos P, Lehrmann DJ, Wei JY, Yu YY, Xiao JF, Chaikin DH, Minzoni M, Berry AK, Montgomery P (2006) Triassic evolution of the Yangtze Platform in Guizhou Province, People’s Republic of China. *Geological Society of America Special Paper* **417**, 1–105.

Ezaki Y, Liu JB, Nagano T, Adachi N (2008) Geobiological Aspects of the earliest Triassic microbialites along the southern periphery of the tropical Yangtze Platform: initiation and cessation of a microbial regime. *Palaios* **23**, 356–369.

Ezaki Y, Liu JB, Adachi N (2012) Lower Triassic stromatolites in Luodian County, Guizhou Province, South China: evidence for the protracted devastation of the marine environments. *Geobiology* **10**, 48–59.

Farabegoli E, Perri MC, Posenato R (2007) Environmental and biotic changes across the Permian–Triassic boundary in western Tethys, the Bulla parastratotype, Italy. *Global and Planetary Change* **55**, 109–135.

Feng ZZ, Bao ZD, Li SW (1997) *Lithofacies Paleogeography of Early and Middle Triassic of South China*. Petroleum Industry Press, Beijing, pp. 1–222 (in Chinese).

Friedman GM, Shukla AV (1980) Significance of authigenic quartz euhedra after sulfates: example from the Lockport Formation (Middle Silurian) of the New York. *Journal of Sedimentary Research* **50**, 1299–1304.

García Delcura MA, Salvador Ordóñez JC, Jones BF, Cañaveras JC (2001) Petrology and geochemical evidence for the formation of primary bacterially induced lacustrine dolomite: La Roda 'white earth' (Pliocene, central Spain). *Sedimentology* **48**, 897–915.

Gregg JM, Howard SA, Mazzullo SJ (1992) Early diagenetic recrystallization of Holocene (<3000 years old) peritidal dolomites, Ambergris Cay, Belize. *Sedimentology* **39**, 143–160.

Hips K, Haas J (2006) Calcimicrobial stromatolites at the Permian–Triassic boundary in a western Tethyan section, Bükk Mountains, Hungary. *Sedimentary Geology* **185**, 239-253.

Hu SX, Zhang QY, Chen ZQ, Zhou CY, Lv T, Xie T, Wen W, Huang JY, Benton MJ (2011) The Luoping biota: exceptional preservation, and new evidence on the Triassic recovery from end-Permian mass extinction. *Proceedings of the Royal Society, Series B* **278**, 2274–2283.

Kah LC, Riding R (2007) Mesoproterozoic carbon dioxide levels inferred from calcified cyanobacteria. *Geology* **35**, 799–802.

Kaźmierczak J, Altermann W (2002) Neoarchean biomineralization by benthic cyanobacteria. *Science* **298**, 2351.

Kaźmierczak J, Kempe S, Kremer B, López-García P, Moreira D, Tavera R (2011) Hydrochemistry and microbialites of the alkaline crater lake Alchichica, Mexico. *Facies* **57**, 543–570.

Kershaw S, Li Y, Crasquin-Soleau S, Feng QL, Mu XN, Collin P, Reynolds A, Guo L (2007) Earliest Triassic microbialites in the South China block and other areas: controls on their growth and distribution. *Facies* **53**, 409–425.

Kershaw S, Crasquin S, Collin PY, Li Y, Feng QL, Forel MB (2009) Microbialites as disaster forms in anachronistic facies following the end-Permian mass extinction: a discussion. *Australian Journal of Earth Sciences* **56**, 809–813.

Kershaw S, Crasquin S, Forel MB, Randon S, Collin PY, Kosun E, Richoz S, Baud A (2011) Earliest Triassic microbialites in Çürük Dag, southern Turkey: composition, sequence and controls on formation. *Sedimentology* **58**, 739–755.

Kershaw S, Crasquin S, Li Y, Collin PY, Forel MB, Mu XN, Baud A, Wang Y, Xie SC, Maurer F, Gou L (2012) Microbialites and global environmental change across the Permian–Triassic boundary: a synthesis. *Geobiology* **10**, 25–47.

Krause S, Liebetrau V, Gorb S, Sánchez-Román M, Mckenzie J, Treude T (2012) Microbial nucleation of Mg-rich dolomite in exopolymeric substances under anoxic modern seawater

salinity: new insight into an old enigma. *Geology* **40**, 587–590.
Li F, Yan JX, Algeo T, Wu X (2012) Paleoceanographic conditions following the end-Permian mass extinction recorded by giant ooids (Moyang, South China). Global and Planetary Change doi:10.1016/j.gloplacha.2011.09.009.
Mary ML, Woods AD (2008) Stromatolites of the Lower Triassic Union Wash Formation, CA: evidence for continued post-extinction environmental stress in western North America through the Spathian. *Palaeogeography, Palaeoclimatology, Palaeoecology* **261**, 78–86.
Mastandrea A, Perri E, Russo F, Spadafora A, Tucker M (2006) Microbial primary dolomite from a Norian carbonate platform: northern Calabria, southern Italy. *Sedimentology* **53**, 465–480.
Mata SA, Bottjer DJ (2011) Origin of Lower Triassic microbialites in mixed carbonate-siliciclastic successions; ichnology, applied stratigraphy, and the end-Permian mass extinction. *Palaeogeography, Palaeoclimatology, Palaeoecology* **300**, 158–178.
Mata SA, Bottjer DJ (2012) Microbes and mass extinctions: paleoenvironmental distribution of microbialites during times of biotic crisis. *Geobiology* **10**, 3–24.
Oliveri E, Neri R, Bellanca A, Riding R (2010) Carbonate stromatolites from a Messinian hypersaline setting in the Caltanissetta Basin, Sicily: petrographic evidence of microbial activity and related stable isotope and rare earth element signatures. *Sedimentology* **57**, 142–161.
Paul J, Peryt TM (2000) Kalkowsky's stromatolites revisited (Lower Triassic Buntsandstein, Harz Mountains, Germany). *Palaeogeography, Palaeoclimatology, Palaeoecology* **161**, 435–458.
Paul J, Peryt TM, Burne RV (2011) Kalkowsky's stromatolites and oolites (Lower Buntsandstein, northern Germany). In *Advances in stromatolite Geobiology. Lecture Notes in Earth Sciences*. 131 (eds Reitner J, Guéric N-V, Arp G). Springer-Verlag, Berlin, Heidelberg, pp. 13–28.
Peckmann J, Thiel V (2004) Carbon cycling at ancient methane–seeps. *Chemical Geology* **205**, 443–467.
Pentecost A, Bauld J (1987) Nucleation of calcite on sheaths of cyanobacteria using a simple diffusion cell. *Geomicrobiology Journal* **6**, 129–135.
Perri E, Tucker M (2007) Bacterial fossils and microbial dolomite in Triassic stromatolites. *Geology* **35**, 207–210.
Pruss SB, Bottjer DJ, Corsetti FA, Baud A (2006) A global marine sedimentary response to the end-Permian mass extinction: examples from southern Turkey and the western United States. *Earth-Science Reviews* **78**, 193–206.
Renaut RW, Jones B, Tercelin JJ (1998) Rapid in situ silicification of microbes at Loburu hot springs, Lake Bogoria, Kenya Rift Valley. *Sedimentology* **45**, 1083–1103.
Richoz S, Baud A, Krystyn L, Twitchett R, Marcoux J (2005) Permo-Triassic deposits of the Oman Mountains: from basin and slope to the shallow platform. Field Guidebook, 24th IAS Regional Meeting, Oman.
Riding R (2000) Microbial carbonates: the geological record of calcified bacterial-algal mats and biofilms. *Sedimentology* **47**, 179–214.
Riding R, Liang L (2005) Geobiology of microbial carbonates: metazoan and seawater saturation state influences on secular trends during the Phanerozoic. *Palaeogeography, Palaeoclimatology, Palaeoecology* **219**, 105–115.
Riding R (2006) Microbial carbonate abundance compared with fluctuations in metazoan

diversity over geological time. *Sedimentary Geology* **185**, 229–238.
Reid RP, Visscher PT, Decho AW, Stolz JF, Bebout BM, Dupraz C, Macintyre IG, Paerl HW, Pinckney JL, Prufert-Bebout L, Steppe TF, DesMarais DJ (2000) The role of microbes in accretion, lamination and early lithification of modern marine stromatolites. *Nature* **406**, 989-992.
Reid RP, James NP, Macintyre IG, Dupraz C, Burne NRV (2003) Shark Bay stromatolite: microfabrics and reinterpretation of origins. *Facies* **49**, 299–324.
Reitner J, Quéric NV, Arp G (2011) *Advances in stromatolite Geobiology*. Springer, pp. 1–559
Schubert JK, Bottjer DJ (1992) Early Triassic stromatolites as post-mass extinction disaster forms. *Geology* **20**, 883-886.
Saito R, Oba M, Kaiho K, Maruo C, Hujibayashi M, Chen J, Chen ZQ, Tong J (2013) Ether lipids from the Lower and Middle Triassic at Qingyan, Guizhou Province, Southern China. *Organic Geochemistry* (in press).
Sano H, Nakashima K (1997) Lowermost Triassic (Griesbachian) microbial bindstone-cementstone facies southwest Japan. *Facies* **36**, 1–24.
Shapiro RS (2000) A comment on the systematic confusion of thrombolites. *Palaios* **15**, 166–169.
Seong-Joo L, Browne KM, Golubic S (2000) On stromatolite lamination. In *Microbial Sediments* (eds Riding R, Awramik SM). Springer-Verlag, Berlin-Heidelberg, pp. 16–24.
Golubic S, Seong-Joo L, Browne KM (2000) Cyanobacteria: Architects of sedimentary structures. In Microbial Sediments (eds Riding R, Awramik SM). Springer-Verlag, Berlin-Heidelberg, pp. 57–67.
Sun YD, Joachimski MM, Wignall, PB, Yan CB, Chen YL, Jiang HS, Wang LN, Lai XL (2012) Lethally hot temperatures during the Early Triassic greenhouse. *Science* **338**, 366–370.
Wignall PB, Twitchett RJ (2002) Permian–Triassic sedimentology of Jameson Land, East Greenland: incised submarine channels in an anoxic basin. *Journal of Geological Society, London* **159**, 691–703.
Woods AD (2012) Microbial ooids and cortoids from the Lower Triassic (Spathian) Virgin Limestone, Nevada, USA: Evidence for an Early Triassic microbial bloom in shallow depositional environments. *Global and Planetary Change* http://dx.doi.org/10.1016/j.gloplacha.2012.07.011
Woods AD, Bottjer DJ, Mutti M, Morrison J (1999) Lower Triassic large sea-floor carbonate cements: their origin and a mechanism for the prolonged biotic recovery from the end-Permian mass extinction. *Geology* **27**, 645–648.
Wright DT (1999) The role of sulpate-reducing bacteria and cyanobacteria in dolomite formation in distal ephemeral lakes of the Coorong region, South Australia. *Sedimentary Geology* **126**, 147–157.
Wright DT, Wacey D (2005) Precipitation of dolomite using sulphate-reducing bacteria from the Coorong Region, South Australia: significance and implications. *Sedimentology* **52**, 987–1008.
Vasconcelos C, Mckenzie JA (1997) Microbial mediation of modern dolomite precipitation and diagenesis under anoxic conditions (Lagoa Vermelha, Rio de Janeiro, Brazil). *Journal of Sedimentary Research* **67**, 378–390.
Vasconcelos C, Mckenzie JA, Bernasconi S, Grujic D, Tien AJ (1995) Microbial mediation as

a possible mechanism for natural dolomite formation at low temperature. *Nature* **377**, 220–222.
Visscher PT, Stolz JF (2005) Microbial mats as bioreactors: populations, processes, and products. *Palaeogeography, Palaeoclimatology, Palaeoecology* **219**, 87–100.
Visscher PT, Reid RP, Bebout BM, Hoeft SE, Macintyre IG, Thompson JA (1998) Formation of lithified micritic laminae in modern marine stromatolites (Bahamas): The role of sulphur cycling. *American Mineralogist* **83**, 1482–1493.
Yang H, Chen ZQ, Wang YB, Tong JN, Song HJ, Chen J (2011) Composition and structure of microbialite ecosystems following the end-Permian mass extinction in South China. *Palaeogeography, Palaeoclimatology, Palaeoecology* **308**, 111–128.
Zhang QY, Zhou CY, Lu T, Xie T, Lou XY, Liu W, Sun YY, Wang XS (2008) Discovery and significance of the Middle Triassic Anisian Biota. *Geological Review* **54**, 523–527 (in Chinese with English abstract).
Zhang QY, Zhou, CY, Lu T, Xie T, Lou XY, Liu W, Sun YY, Huang JY, Zhao LS (2009) A conodont-based Middle Triassic age assignment for the Luoping Biota of Yunnan, China. *Science in China Series D: Earth Sciences* **52**, 1673−1678.
Zhao XM, Tong JN, Yao HZ, Zhang KX, Chen ZQ (2008) Anachronistic facies in the Lower Triassic of South China and their implications to the ecosystems during the recovery time. *Science in China Series D: Earth Sciences* **51**, 1646–1657.

Figure captions

Fig. 1 Locality of the studied Shangshikan section in Luoping County, eastern Yunnan Province, SW China (base map follows Zhang *et al.*, 2009).

Fig. 2 Columnar section of Member II of the Guanling Formation exposed at the Shangshikan section showing the Luoping stromatolite horizon and field photos showing macro-structures of the stromatolites. (A) Field view showing domal structures and laminae in stromatolite; hammer is 35 cm long. (B) Upright, branching stromatolite columns. (C) Polished slab showing domal and columnar stromatolite structures and pronounced alternations of dark and light colored laminae. Note area **a** was sampled for SEM microanalysis, while area **b** was sampled for thin section observation. (D) Horizontal view of stromatolite columns. Note columns preserved as rounded reliefs (indicated by white arrow). (E) Close-up of columns in D on a polished slab showing spheroidal structures.

Fig. 3 Photomicrographs of non-stromatolite facies. (A) Dolomitic wackestone facies below domal stromatolites. Note bioclasts were usually recrystallized and altered to coarse dolomite. (B, C) Interstromatolite oncoidal wackestone-packstone facies with distinct oncoids and bivalve and foraminiferal fragments. (D) Bioclastic packstone-wackestone facies overlying the domal stromatolites. All scale bars are 1 mm.

Fig. 4 Photomicrographs of the Luoping stromatolites. (A) Thin sectioned area of b in **Fig. 2**C. Note the domal structures defined by well-preserved laminations, with dark

colored laminae alternating with light colored laminae. Dotted line represents the boundary between domal stromatolitic bindstone and the overlying oncoidal packstone. (B) Close up of area **a** (in Fig. 4A) showing the upright, thin filaments and fenestrae represented by small, rounded holes in dark laminae of stromatolite. (C) Close up of rectangular area in Fig. 4B showing both upright filaments in life position (white arrow indicated) and fenestrae (black arrow indicated). (D) Close up of area **b** (in Fig. 4A) showing oncoidal packstone of stromatolite-capping facies. Note irregular bioclasts were coated with micrite. (E) Bioclastic packstone-wackestone of stromatolite-capping facies showing irregularly shaped clotted structures and bioclasts.

Fig. 5 Photomicrographs of the Luoping stromatolites. (A) Close up of area c in **Fig. 4**A showing the well-preserved filamentous cyanobacterial colony comprising individual upright filaments in life position (indicated by white arrows) and fenestrae represented by circular holes (black arrows) in dark laminae. (B, C) Close up of individual upright filaments and filament shealth in dark laminae. (D) Close up of area d in **Fig. 4**A showing that the clotted fabrics formed erratic filaments consortia and that filaments were arranged prostrate. (E, F) Close up of central area in D showing prostrate filament shealth.

Fig. 6 Clotted fabric and micritization in dark laminated area of stromatolites in transmitted light and epifluorescent light. (A) Irregularly clotted fabrics are composed of filaments in stromatolites. (B, C) The same area as that in Fig. 6A but captured by fluorescent microscope. Note the strong autofluorescent area in B and C are closely associated with clotted filaments. (D, E, F) Another view of filaments and clotted fabrics in dark laminae of stromatolite. Although filaments were weakly defined in transmitted light image (D), strong autofluorescence were also observed in proximity with micrites. Coarsely grained dolomite cement (defined by green light) was poorly responded to fluorescent light (E, F). Note B and E were captured under blue exciting light (wavelength 450–490 nm) while C and F under green exciting light (wavelength 510–560 nm).

Fig. 7 SEM images of micro-fabric and bacteria forms detected in dark laminae of the Luoping stromatolites. (A) Floating dolomite rhombs on carbonate matrix. (B–D) Individual rods and rod aggregates. Note the interpenetrating feature of rods are shown in Fig. 7D. (E) Dark laminated area in stromatolite showing well-preserved pores. (F) Close up of rectangular area in E showing the interpenetrating rods within the pores. (G) Coccoid structures composed of micron-sized dolomite rhombs. (H) Spherical bodies that coexisted with rods in dark laminae. E, F and H were backscattered electron images, the rest were secondary electron images. Samples for SEM imaging were etched with HCl.

Fig. 8 Close up of an individual rod in the pore under SEM. Rod in the centre area has a shealthed outer layer, which is 2 μm thick. The centre of rod was filled with coarse dolomite crystals. Note the nano-sized dolomite rhombs (white arrows indicated) were stuck on rod during the preliminary phase of the growth.

Fig. 9 SEM images showing thin biofilms and fibrous slime in contact with minute dolomite and rod aggregates. (A) A thin slime of biofilm covered minute rhombic dolomite crystal. (B) Mucilaginous fibers (white arrow indicated) contacting various dolomite grains. (C) Mucilaginous fibers coalescing rod aggregates. (D) Close-up of upper rectangular area in Fig. 9C showing minute dolomite grains composing a rod shape. (E) Close-up of lower rectangular area in Fig. 9C showing filamentous biofilms (white arrows indicated) that contacted minute dolomite rhombs. (F) Euhedral quartz grains with double terminations in contact with minute dolomite grains (white arrows indicated). Note the rills (black arrow indicated) are pronounced on surface of quartz crystals.

Fig. 10 EDS analytical results of three different components of dolomite grains in the Luoping stromatolites. White cross corresponds to analyzing point. Element Au indicates goad coating of samples. (A) Floating dolomite grains that showed a composition of Ca dolomite (showed by EDS spectrum in a), with few percentage of element Si. (B) Rod covered with minute dolomite rhomb, which showed small percentage of element Si in composition (showed by EDS spectrum in b).

Fig. 1

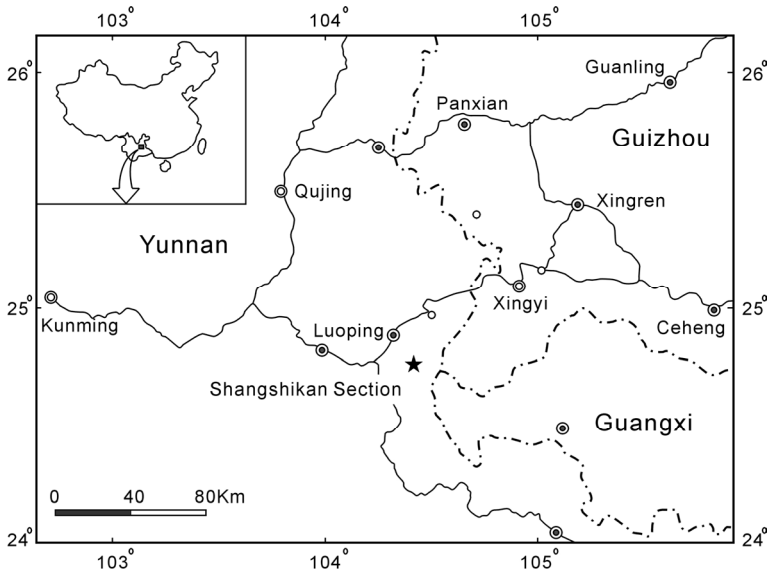
103°
104°
105°
26°
25°
24°
Guanling
Panxian
Guizhou
Qujing
Xingren
Yunnan
Xingyi
Kunming
Luoping
Ceheng
Shangshikan Section
Guangxi
0
40
80Km

Fig. 2

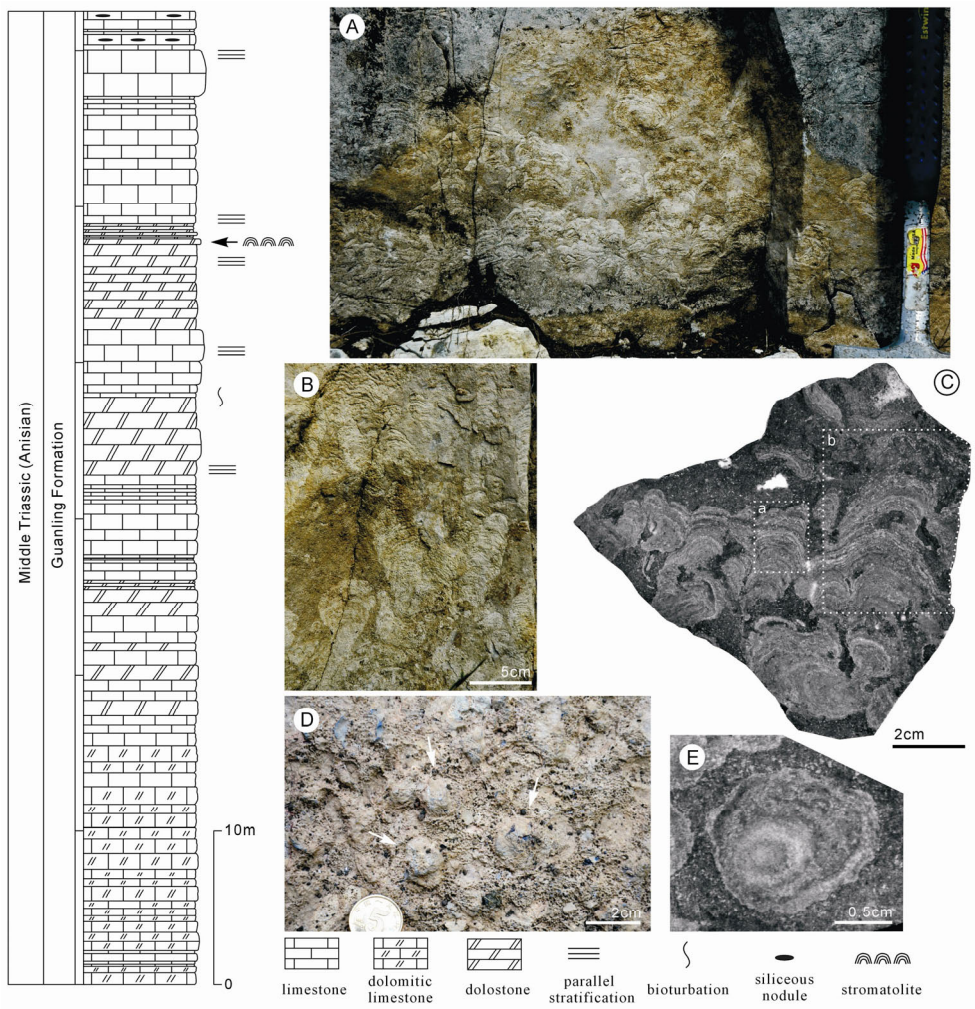
Middle Triassic (Anisian)
Guanling Formation
10m
0
A
B
5cm
C
a
b
2cm
D
2cm
E
0.5cm
limestone
dolomitic limestone
dolostone
parallel stratification
bioturbation
siliceous nodule
stromatolite

Fig. 3

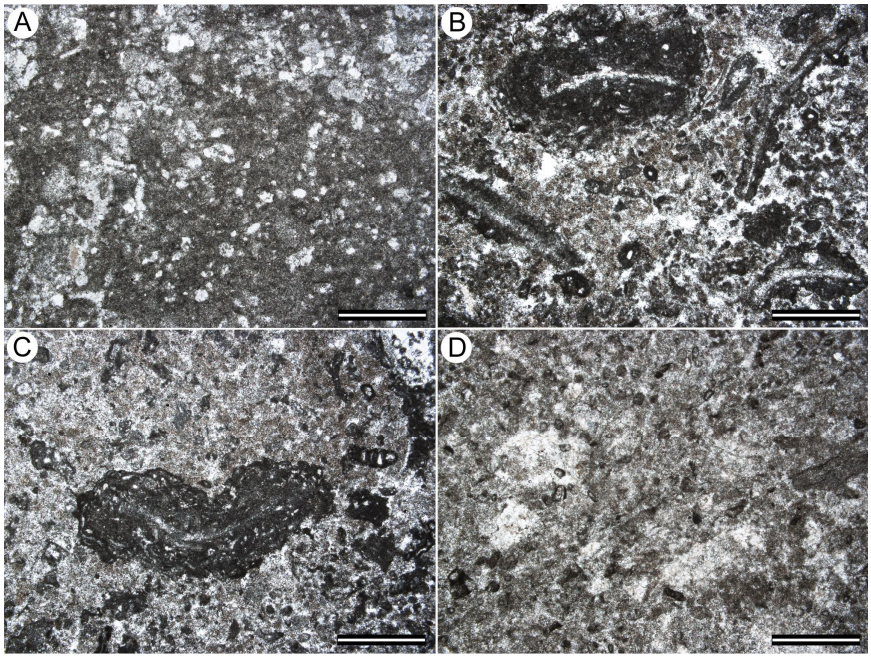

Fig. 4

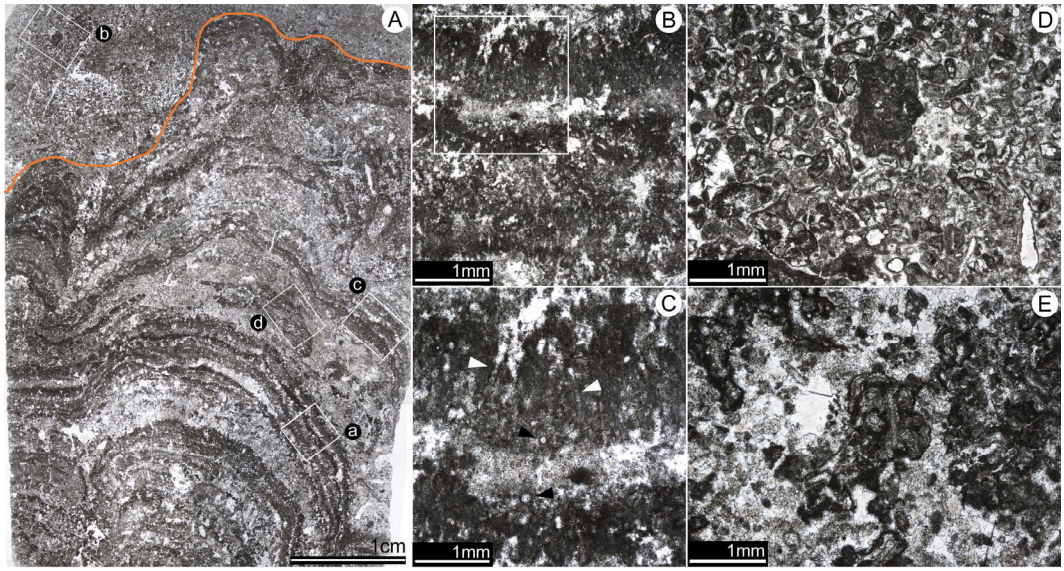

Fig. 5

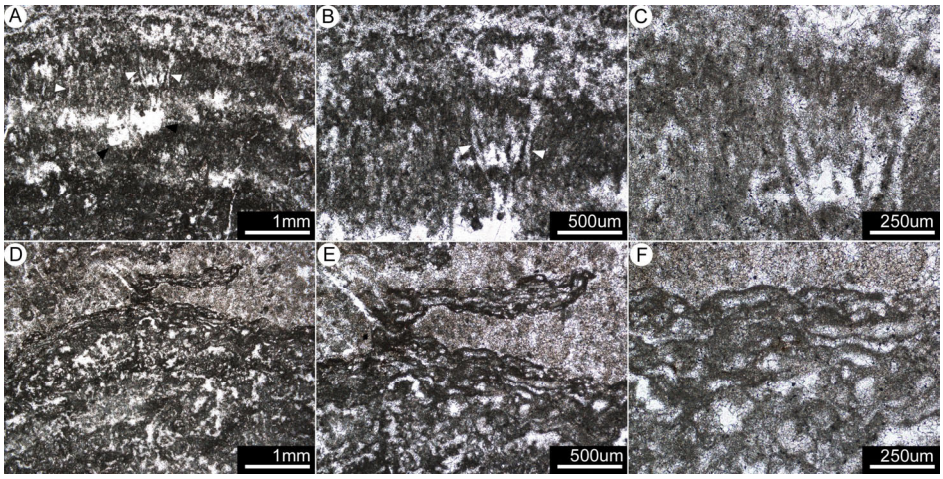

Fig. 6

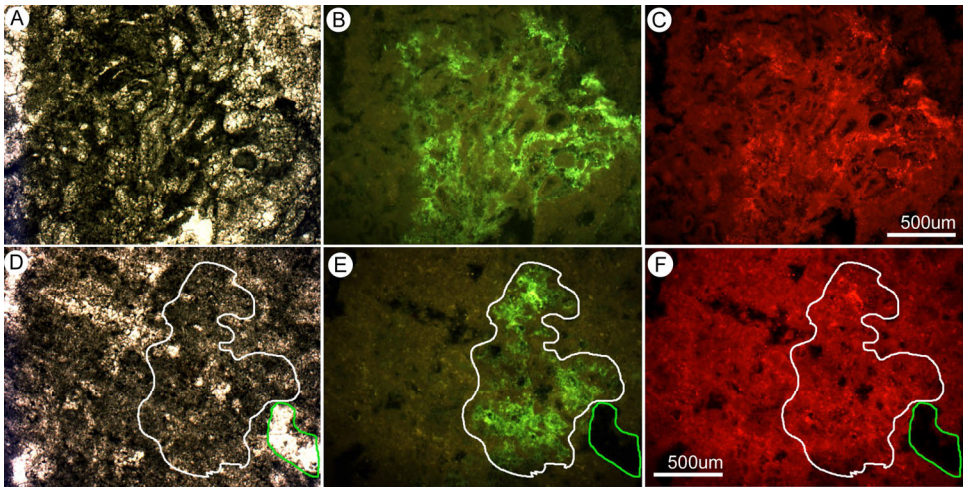

Fig. 7

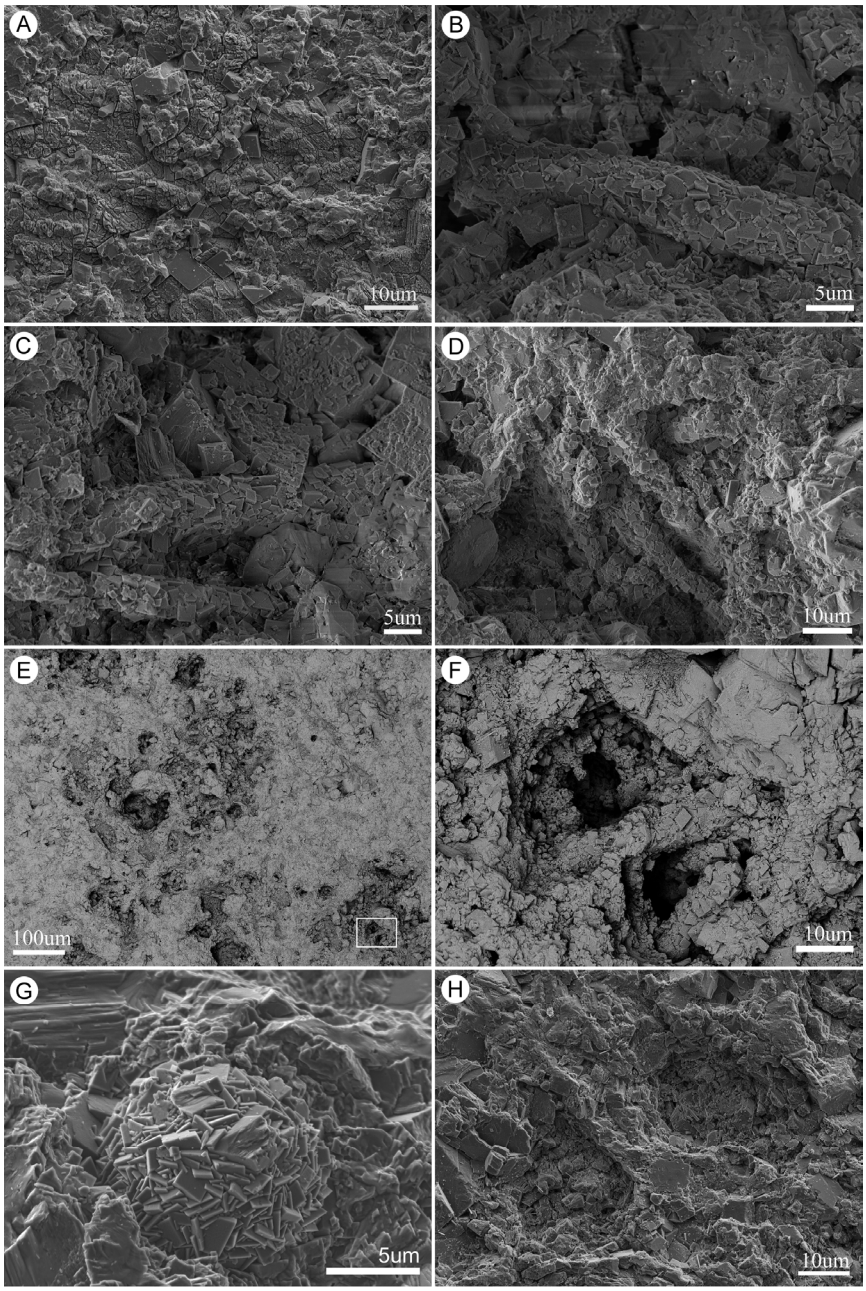

Fig. 8

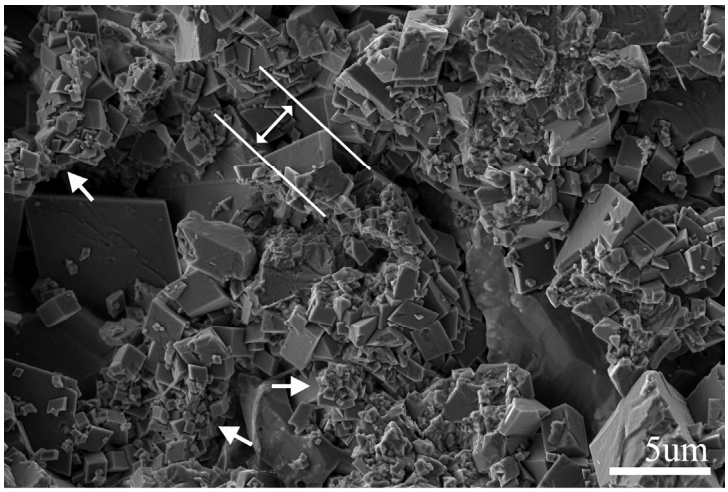

Fig. 9

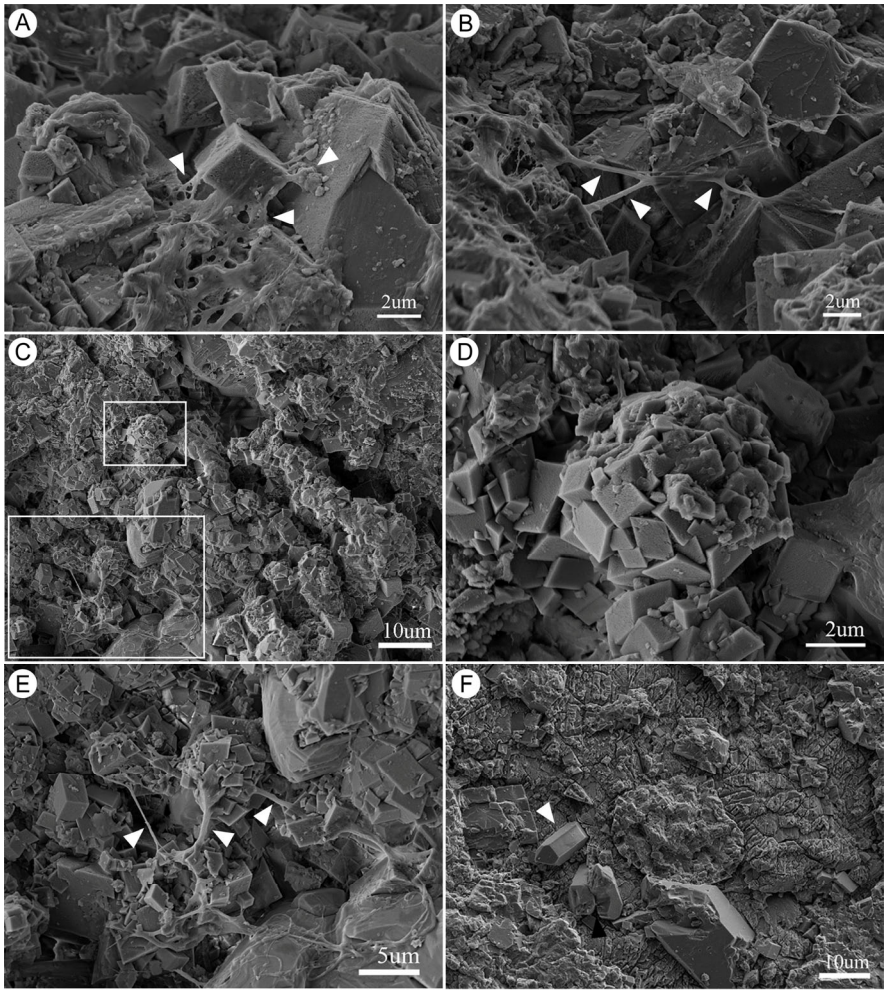

Fig. 10

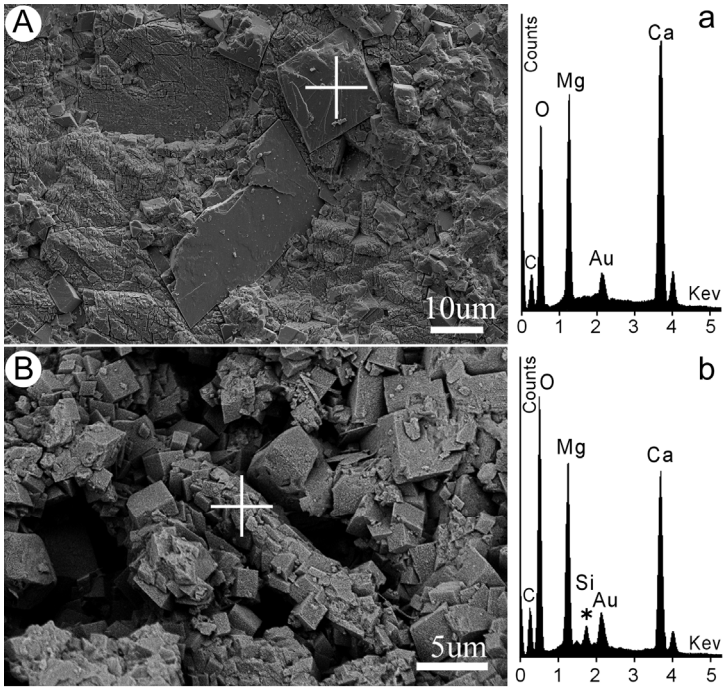
A
10um
a
Counts
Ca
Mg
O
C
Au
Kev
0 1 2 3 4 5
B
5um
b
Counts
O
Mg
Ca
C
Si
Au
*
Kev
0 1 2 3 4 5